Chinese Chemical Letters 34 (2023) 107933

Contents lists available at ScienceDirect

Chinese Chemical Letters

journal homepage: www.elsevier.com/locate/cclet

Antioxidant induced bulk passivation for efficient and stable hole transport layer-free carbon electrode perovskite solar cells

Yetai Cheng[a], Qingbo Wei[a,*], Nannan Wang[a], Zhangwen Ye[a], Yanbin Zhao[a], Qiongyao Wang[a], Depeng Chu[b], Lingxing Zan[a], Feng Fu[a,*], Yucheng Liu[b,*]

[a] Key Laboratory of Chemical Reaction Engineering of Shaanxi Province, College of Chemistry & Chemical Engineering, Yan'an University, Yan'an 716000, China

[b] Shaanxi Key Laboratory for Advanced Energy Devices, Shaanxi Engineering Lab for Advanced Energy Technology, Institute for Advanced Energy Materials, School of Materials Science and Engineering, Shaanxi Normal University, Xi'an 710062, China

ARTICLE INFO

Article history:
Received 4 July 2022
Revised 7 October 2022
Accepted 18 October 2022
Available online 25 October 2022

Keywords:
Perovskite solar cells
Additive engineering
Defect passivation
Long-term stability
Carbon electrode

ABSTRACT

Defect passivation is one of the important strategies to improve the efficiency and stability of perovskite solar cells. In this work, 2,6-di–*tert*–butyl–4-methylphenol (BHT) as antioxidant was introduced into the perovskite precursor solution to improve the quality of the prepared perovskite films, so that these films performed a larger and uniform grain size. Moreover, the –OH functional group in BHT interacts with I^-, thus reducing the density of defect states and inhibiting the non-radiative recombination. The presence of hydrophobic groups in BHT protects the film from moisture erosion and improves the long-term stability of PSCs devices. The maximum photoelectric conversion efficiency of the constructed ITO/SnO_2/BHT-$MAPbI_3$/Carbon device is 16.88%, and the unpackaged cell maintains the initial efficiency of 99.3% after 698 h of storage under the environmental condition of 30% humidity. This work provides an efficient approach to improve the performance of printable hole transport layer-free carbon electrode perovskite solar cells.

Organic-inorganic hybrid perovskite solar cells (PSCs) have received widespread attention from both academic and commercial owning to their excellent optoelectronic properties, such as large light absorption coefficient, long carrier diffusion length, low defect density, and low exciton binding energy [1–6]. Its power conversion efficiency (PCE) has increased rapidly from 3.8% to 25.7% after over ten years of development, and has reached a level comparable to that of commercial polycrystalline silicon solar cells [7,8]. However, conventional PSCs still suffer from some issues, such as low efficiency and poor stability. Noble metal electrodes (Au and Ag) and organic hole transport layer (HTL) in the conventional PSCs devices interact with the halide perovskite layers to destabilize the PSCs [9]. Perovskite films can be easily decomposed under the action of environmental factors such as oxygen, moisture, and light [10].

To address the negative effects of metal electrodes and HTL on the device, the researchers constructed HTL-free C-PSCs, whose PCE has risen from 6.64% to 18.9% [11]. The device prevents the effect of metal electrodes and HTL on the perovskite layer, while the hydrophobic and inexpensive carbon electrodes resulted in improving device stability and lower fabrication costs. Unfortunately, the HTL-free C-PSCs also have some shortcomings, such as low energy band matching between the perovskite layer and the carbon electrode, insufficient contact, and several defects which hinder hole transport between the perovskite layer and the carbon electrode, leading to severe nonradiative complexation and degradation of device photovoltaic performance [12,13]. In addition, one of the main reasons for the susceptibility of perovskite films to performance degradation under environmental conditions is that solution-processed perovskite films have a large number of defect sites (under-coordinated Pb^{2+} and I^-, *etc.*) at the surface or grain boundaries [14,15]. These defect sites often act as centers for unexpected non-radiative recombination, thereby limiting further improvement in the photovoltaic performance and stability of PSCs [16,17]. Therefore, reducing defect sites in perovskite films and obtaining high-quality perovskite/carbon interfaces have become one of the important factors for enhancing the performance of the devices.

In recent years, additive engineering has been widely used to reduce the film defects, improving the quality of perovskite films [18–20]. For example, Zou *et al.* [21] added ethylamine al-

* Corresponding authors.
E-mail addresses: qbwei@yau.edu.cn (Q. Wei), fufeng@yau.edu.cn (F. Fu), liuyc@snnu.edu.cn (Y. Liu).

https://doi.org/10.1016/j.cclet.2022.107933
1001-8417/

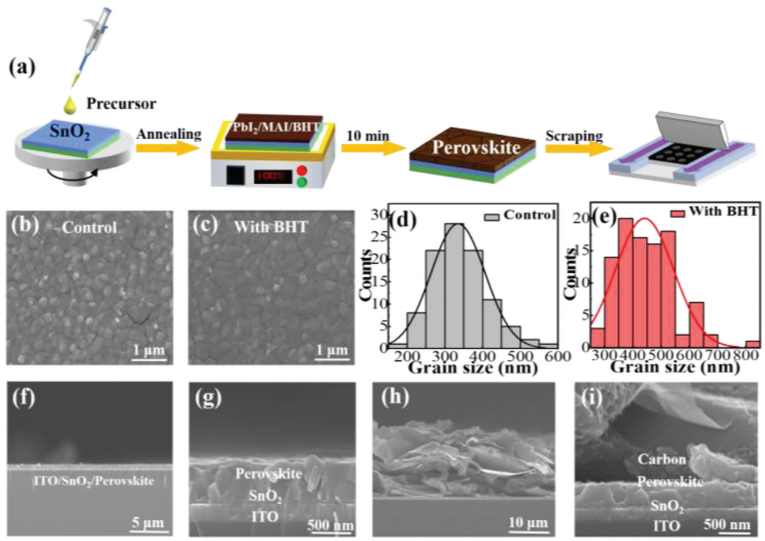

Fig. 1. (a) Schematic diagram of the preparation process of BHT-$MAPbI_3$-based perovskite solar cells. (b, c) Top-view SEM images and (d, e) grain size statistics charts of perovskite films with/without BHT. (f, g) Cross-sectional SEM images of the $MAPbI_3$-perovskite film and (h, i) ITO/SnO_2/Perovskite/Carbon solar cell device.

cohol chlorides to the perovskite precursor solution, and found that −OH and $-NH_3^+$ passivated the defects by immobilizing the halide anion in perovskite through hydrogen bonding or by coordination with the undercoordinated I^-, thus passivating the defects and increasing the device conversion efficiency from 14.52% to 16.97%. Park *et al.* [22] used the −SH group in (3-mercaptopropyl) trimethoxysilane to interact with PbI_2 *via* Lewis acid-base, obtaining the perovskite films with a larger grain size and extending the carrier lifetime, which improved the wet stability and thermal stability of the devices. Pan *et al.* [23] reduced the charge defects generated in perovskites and constructed the cells with excellent environmental stability by introducing halogen functional groups (−F and −Cl) in passivating molecules. Guo *et al.* [24] reported that the $-NH_2$ and −COOH functional groups in ploy-L-lysine had a strong chelating effect with the undercoordinated Pb^{2+}, which passivated the Pb-I inversion defect and significantly increased the open-circuit voltage, thus increasing the device efficiency up to 19.45%. Meng *et al.* [25] effectively promoted the growth of perovskite crystals by a bifunctional additive composed of organic ammonium cation and dithiocarbamate anions, and the constructed devices could still maintain 90% of the initial efficiency after 500 h of continuous operation. Although the functionalized additives play a significant role in passivating defects, the selection of the optimized additive remains a challenge.

In this work, we added the 2,6-di–*tert*–butyl–4-methylphenol (BHT) containing benzene rings and hydroxyl groups into the precursor solution to prepare high quality perovskite films. The benzene ring in BHT has a rigid structure and strong π-π bonding interactions with high binding energy [26], which leads to its aggregation near the perovskite grain boundaries and planes during film formation, reducing the free energy barrier for nucleation within the grain boundaries and promoting the growth of perovskite in the grain boundaries [27]. The hydroxyl group in BHT can suppress the ion migration in the perovskite film through the strong hydrogen bond between −H and I ion [28,29]. The ITO/SnO_2/BHT-$MAPbI_3$/Carbon cell was constructed to further demonstrate that BHT improves the HTL-free C-PSCs performance. The PCE of the BHT-$MAPbI_3$-based champion device is significantly improved to 16.88% compared to the pristine device with a PCE of 12.16%. And the unpackaged BHT-$MAPbI_3$-based device retained 99.3% of its initial efficiency after 698 h of storage at ambient conditions with constant humidity of 30%.

Fig. 1a shows the fabrication process of the phenolic antioxidant BHT-$MAPbI_3$-based perovskite solar cells. The different contents of the BHT (Figs. S1 and S2 in Supporting information show the molecular structure and H nuclear magnetic resonance spectra of BHT.) was added into the $MAPbI_3$ precursor solution. The BHT-$MAPbI_3$ perovskite thin film was assembled by spin coating using the prepared precursor solution. Then, carbon electrodes were scraped on the film surface to construct the device.

To investigate the effect of BHT on the morphology of the obtained perovskite films, scanning electron microscopy (SEM) tests were performed. Figs. 1b-e and Fig. S3 (Supporting information) show the top-view SEM images and grain size statistics of the perovskite films without/with BHT. The surface of the perovskite films prepared in the BHT-added solution had a smoother surface, more uniform grain distribution and larger average grain size (control: 340 nm, with BHT: 440 nm) compared with the pristine perovskite films. The π-π bond force of benzene ring gathered of BHT near grain boundaries and crystals, and hydrogen bond cross-linked adjacent grains together, which promoted the growth of perovskite grains to form a larger grain size and increased the surface coverage [30,31]. The high quality of the perovskite films is beneficial to reducing the non-radiative recombination, and improving carrier transport and extraction. Figs. 1f-i show the cross-sectional SEM images of the perovskite film and BHT-$MAPbI_3$-based PSC. The device consisted of ITO/SnO_2 (~40 nm)/BHT-$MAPbI_3$ (~500 nm)/carbon (~15 μm), which the perovskite layer grains were dense and uniform. In addition, each layer of the device was closely stacked with good contact, which is conducive to reducing interfacial charge recombination. Fig. S4 (Supporting information) shows the energy-dispersive X-ray spectroscopy (EDS) images of the BHT-based perovskite film. EDS mapping shows that BHT was successfully added into the perovskite film, and C, N, Pb, I, and O elements were uniformly distributed within the perovskite film.

As shown in Fig. 2a, the effect of BHT on the crystallinity of $MAPbI_3$ perovskite films was investigated by X-ray diffraction (XRD) patterns. All these films exhibited obvious diffraction peaks at 14.02°, 28.38° and 31.82°, corresponding to the (110), (220) and (310) crystal planes of the cubic structured perovskite. No other diffraction peaks appeared, indicating that the antioxidant BHT did not influence the crystal structure of perovskite, and BHT molecules were bonded at the grain boundaries and surfaces of the perovskite films [32,33]. However, the XRD patterns of the films

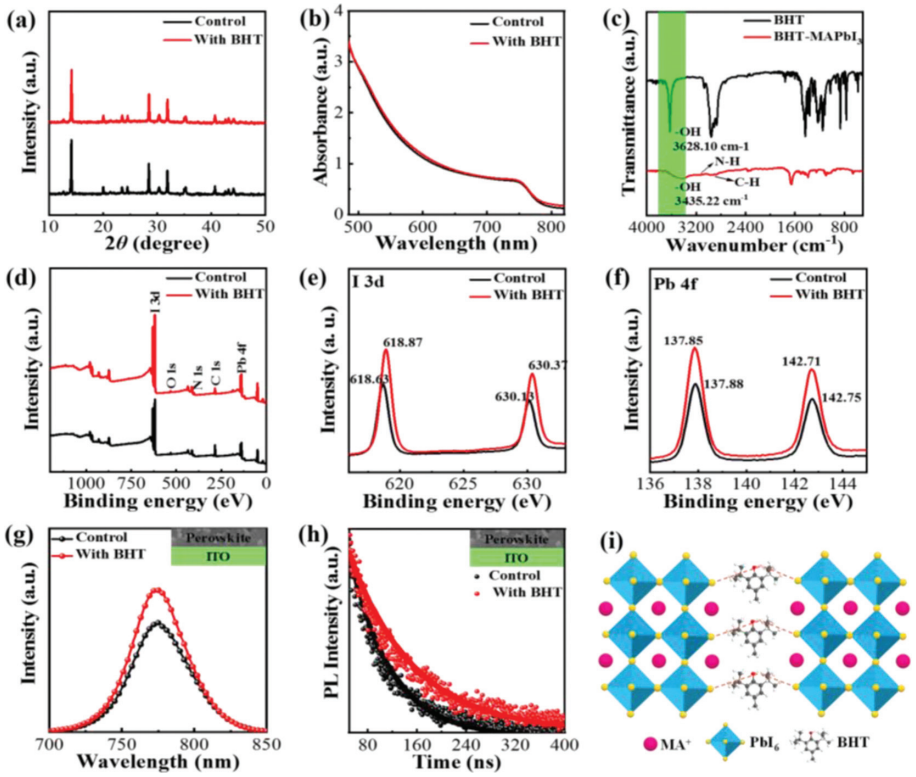

Fig. 2. (a) XRD patterns and (b) UV–vis-NIR spectra of perovskite films with/without BHT. (c) FTIR spectra of BHT and BHT-$MAPbI_3$. (d-f) XPS spectra and of perovskite films with and without BHT. (g, h) PL and TRPL spectra of ITO/$MAPbI_3$ and ITO/BHT-$MAPbI_3$ perovskite films. (i) Mechanism diagram of the interaction between BHT and $MAPbI_3$ perovskite.

showed weak PbI_2 peaks, attributing to the residual PbI_2. According to the relevant literature reports, the existence of traces of PbI_2 in the perovskite film is beneficial to improving the device performance and stability [34,35].

The effect of BHT on the optical absorption of $MAPbI_3$ perovskite films was investigated by UV–vis-NIR spectra. Fig. 2b shows that all the absorption band edges of the perovskite films are around 780 nm. Therefore, the contribution of BHT additives to the optical absorption intensity of perovskite films is negligible. The improvement in J_{SC} of ITO/SnO_2/BHT-$MAPbI_3$/C cells may be mainly due to the BHT additives, which can passivate the surface defects, inhibit carrier recombination and promote the hole-electron separation rate [36,37].

The Fourier transform infrared spectroscopy (FTIR) was performed to explore the information of the fresh formed bonding in the $MAPbI_3$ precursor solution, and the FTIR spectra are shown in Fig. 2c. The wavenumbers at 2900–3000 cm^{-1}, 3100–3200 cm^{-1}, and 3435.22 cm^{-1} are related to the stretching vibrations of C–H, N–H, and O–H, respectively [38–40]. The O–H stretching vibration shifted from 3628.10 cm^{-1} (BHT) to 3435.22 cm^{-1} (BHT-$MAPbI_3$), probably due to the interaction of –OH with I^- through hydrogen bonding [41].

Figs. 2d-f and Fig. S5 (Supporting information) show the X-ray photoelectron spectra (XPS) of the perovskite films. For the I 3d spectrum, the characteristic peaks of I $3d_{3/2}$ and I $3d_{5/2}$ located at the binding energy of 630.13 eV and 618.63 eV, respectively. After adding BHT, the binding energy of I $3d_{3/2}$ and I $3d_{5/2}$ shifted to 630.37 eV and 618.87 eV. The binding energy of Pb 4f is almost unchanged. The reason for the shift in the binding energy was speculated that it owes to the change of electron cloud density of I^-, indicating the strong electrostatic interaction between I^- with –OH functional group in BHT [42,43], which can passivate the surface defects of the perovskite films and inhibit the charge recombination [44,45].

Figs. 2g and h shows the PL and TRPL of the perovskite films. The $MAPbI_3$ and BHT-$MAPbI_3$ films showed an obvious peak at 775 nm, and the BHT-$MAPbI_3$ film possessed a higher PL intensity. We calculated the carrier lifetime (Table S1 in Supporting information) from the TRPL spectrum in Fig. 2h. The carriers of the perovskite film have a longer average lifetime (with BHT: 24.81 ns, control: 16.58 ns). The PL and TRPL results indicate that BHT passivated the film defects, and effectively improved the optoelectronic performance of the device [46,47]. The interaction between $MAPbI_3$ perovskite and BHT is further shown as in Fig. 2i.

The ITO/SnO_2/perovskite/carbon devices were further constructed to study the effect of BHT on photovoltaic performance and the device structure is shown in Fig. 3a. Fig. 3b and Table 1 show the *J-V* curves and photovoltaic parameters of the ITO/SnO_2/BHT-$MAPbI_3$/Carbon champion cells constructed with different contents of BHT. The values of PCE, V_{OC}, J_{SC}, FF of $MAPbI_3$-based perovskite solar cell were determined to be 12.16%, 1.07 V, 18.37 mA/cm^2, and 62.08%, respectively. When the content of BHT was increased to 25 mmol/L, the BHT-$MAPbI_3$-based perovskite solar cell exhibited outstanding performance with a PCE of 16.88%, V_{OC} of 1.12 V, J_{SC} of 22.97 mA/cm^2, and FF of 65.66%. Afterwards, the device efficiency decreased rapidly with the further increase in the BHT content. As listed in Table 1, the PCE of BHT-$MAPbI_3$-based perovskite solar cell was dropped to 8.42% with a further in-

Table 1
The *J-V* curves and photovoltaic parameters of the ITO/SnO_2/BHT-$MAPbI_3$/Carbon champion cells constructed with different contents of BHT.

Sample	V_{OC} (V)	J_{SC} (mA/cm^2)	FF(%)	PCE (%)	R_{sh}(Ω)	R_s(Ω)
Control	1.07	18.37	62.08	12.16	4641.8	17.1
12.5 mmol/L	1.09	21.71	61.24	14.53	3726.5	27.2
25 mmol/L	1.12	22.97	65.66	16.88	4751.5	16.7
37.5 mmol/L	1.07	18.49	51.88	10.30	3273.2	56.8

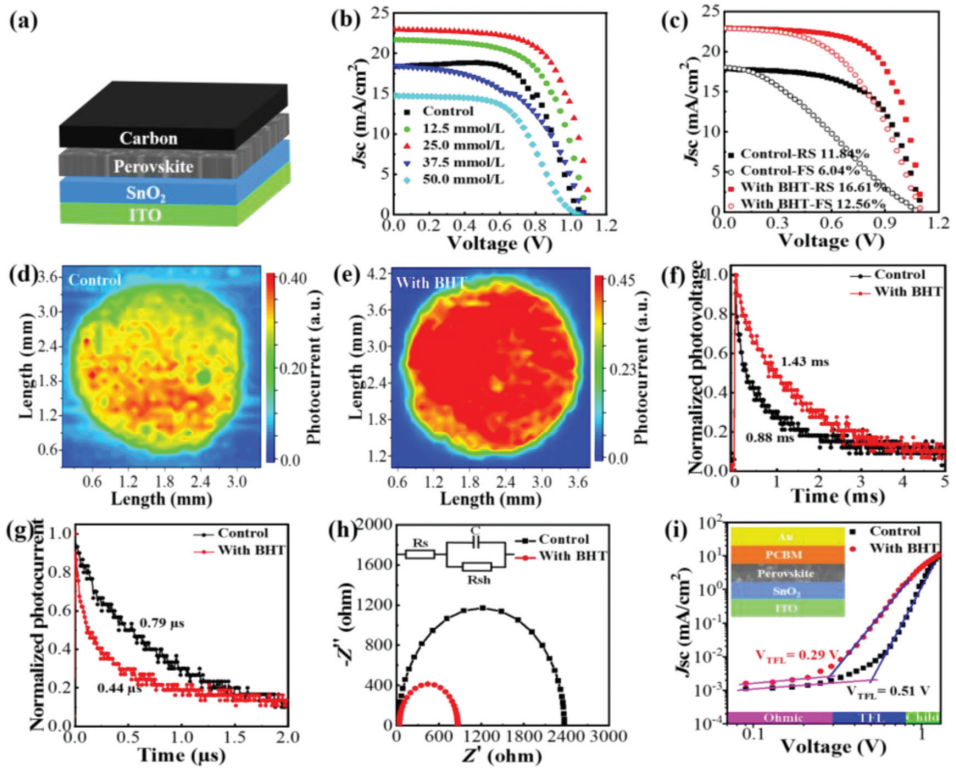

Fig. 3. (a) The structure of ITO/SnO_2/perovskite/carbon PSCs. (b) *J-V* curves of champion PSCs with different contents of BHT. (c) Reverse (forward) scan *J-V* curves, (d, e) photocurrent mapping, (f) transient voltage, (g) transient photocurrent and (h) Nyquist plots of PSCs with/without BHT. (i) Dark *J-V* curves of perovskite films with/without BHT for the ITO/SnO_2/perovskite/PCBM/Au PSCs.

crease in the BHT content upto 50 mmol/L. Therefore, the moderate content of BHT introduced in the precursor solution can effectively improve the photovoltaic performance of the devices.

Fig. 3c and Table 2 show the reverse (forward) *J-V* scan curves and corresponding photovoltaic parameters of perovskite cells with/without BHT, respectively. The reverse (forward) *J-V* tests of the ITO/SnO_2/$MAPbI_3$/Carbon cell suggested a PCE of 11.84 (6.04)%, V_{OC} of 1.12 (1.08) V, J_{SC} of 17.82 (18.05)%, and FF of 59.58 (30.92)%. Interestingly, the reverse (forward) *J-V* tests of the ITO/SnO_2/BHT-$MAPbI_3$/Carbon cell reached a PCE of 16.61 (12.56)%, V_{OC} of 1.11 (1.10) V, J_{SC} of 22.93 (22.93)%, and FF of 65.23 (49.76)%. The results show that BHT can improve the PCE of the cells, and alleviate the hysteresis effect of the devices. The main reason for the retarded hysteresis effect is that the −OH functional group in the additive BHT interacts with I^- *via* hydrogen bond and coordination effect, which inhibits the ion migration. Figs. 3d and e show the photo-current mapping of the device with/without BHT. Compared with the image of the pristine device, the mapping of the device with BHT shows more uniform and higher photocurrent, indicating that BHT passivates the film defects, resulting in a higher J_{SC} [48].

In order to further analyze the carrier dynamics of the device, we tested the transient photovoltage and transient photocurrent decay curves (Figs. 3f and g). As shown in Fig. 3f, the device with BHT addition (1.43 ms) has a longer photovoltage decay lifetime compared to the pristine devices (0.88 ms), indicating that the amount of defects were reduced and carrier recombination was suppressed on the BHT-treated perovskite film, which is consistent with the results of TRPL test [49–51]. Fig. 3g shows the photocurrent decay lifetimes of 0.79 μs and 0.44 μs for devices with and without BHT. The shorter photocurrent decay lifetimes for the BHT-treated device imply that the introduction of BHT increases the charge transfer rate [52,53]. The electrochemical impedance measurement of the devices were also performed under dark condition at bias voltage of 0.9 V. Fig. 3h shows the Nyquist plots of the device. A smaller arc radius indicates a smaller recombination resistance [54,55]. The BHT-$MAPbI_3$-based perovskite cell exhibited a smaller recombination resistance, indicating that the BHT additive can effectively suppress charge-carrier recombination [56,57].

In addition, we evaluated the trap state density (N_t) of perovskite films with/without BHT using the space-charge-limited-current method. The dark *J-V* curves of ITO/SnO_2/perovskite/PCBM/Au cell devices were tested as shown in Fig. 3i. The trap-filled limit voltage (V_{TFL}) of perovskite films with and without BHT are 0.29 V and 0.51 V, respectively. The N_t can be determined by the V_{TFL} according to the following Eq. 1 [58]:

$$N_t = (2\varepsilon\varepsilon_0 V_{TFL})/(eL^2) \quad (1)$$

where ε is the relative dielectric constant of the perovskite; ε_0 is the vacuum permittivity; V_{TFL} is the trap-filled limit voltage; e is the elementary charge; and L is the thickness of the perovskite film. The N_t of devices with/without BHT were calculated to be 4.09×10^{15} cm^{-3} and 7.20×10^{15} cm^{-3}, respectively. The significant reduction in N_t is beneficial to carrier transport in the devices.

The photovoltaic parameters of 10 PSCs constructed with/without BHT were selected to verify the performance

Table 2
The photovoltaic parameters for reverse (forward) *J-V* scans of perovskite solar cells without/with BHT.

Sample	Direction	V_{OC} (V)	J_{SC} (mA/cm^2)	FF (%)	PCE (%)
Control	Reverse	1.12	17.82	59.58	11.84
	Forward	1.08	18.05	30.92	6.04
With BHT	Reverse	1.11	22.93	65.23	16.61
	Forward	1.10	22.93	49.76	12.56

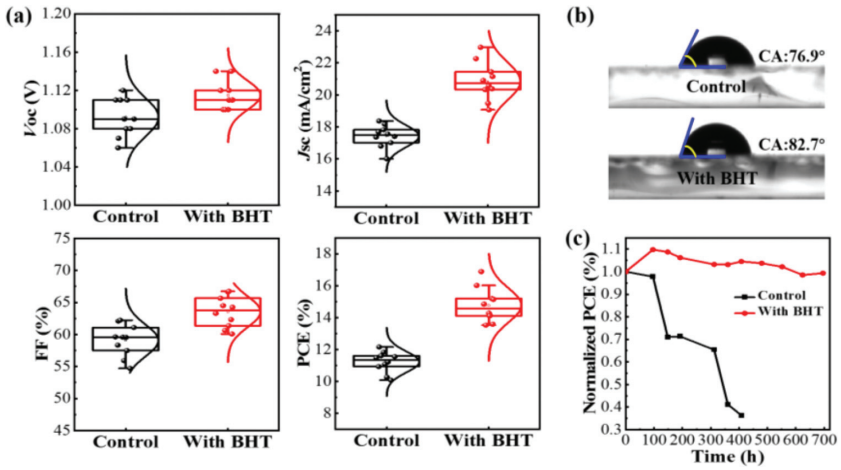

Fig. 4. (a) Statistics of photovoltaic parameters of perovskite solar cells for 10 devices, (b) water contact angle of perovskite films and (c) long-term PCE stability of unpackaged devices under RH of 30% without/with BHT.

reproducibility of ITO/SnO_2/perovskite/carbon cells. Fig. 4a shows the V_{OC}, J_{SC}, FF, and PCE statistics of perovskite solar cells. The PCEs of perovskite cells without BHT were mainly concentrated in 10%–12% (average 11.22%), however, the PCEs of perovskite cells with BHT were mainly concentrated in 14%–16% (average 14.78%). In addition, other photovoltaic parameters (V_{OC}, J_{SC} and FF) of BHT-$MAPbI_3$-based cell devices were improved. The results indicate that moderate BHT can improve the photovoltaic performance and reproducibility of perovskite solar cells under ambient conditions.

Long-term stability is one of the important indicators to evaluate the device performance. Fig. 4b shows the water contact angle (CA) tests of the BHT-$MAPbI_3$-based perovskite films. The average water CA of the perovskite films with/without BHT were 76.0° and 81.9° The effect of the hydrophobic functional group in benzene ring and alkyl groups in BHT can improve the hydrophobicity of the film. Fig. S6 (Supporting information) shows the photos of the perovskite film surface with/without BHT after 56 days, placed in air. It is obvious that BHT can effectively improve the stability of the film. Fig. 4c shows the change of PCE of the unpackaged cells after storage for 698 h in air with a constant humidity of 30%. The PCE of the device without BHT dropped rapidly, whereas the device with BHT maintained 99.3% of the initial PCE after 698 h. The above results indicate that the BHT additive can obviously enhance the long-term stability of the perovskite devices.

In summary, we introduced BHT as an antioxidant into the $MAPbI_3$ perovskite precursor solution, and obtained high-quality perovskite films with large grain size and uniform distribution under ambient conditions, which accelerated the carrier transport and extraction rates. The results indicate that the BHT-added perovskite solar cells exhibited excellent photovoltaic performance and high stability. Compared with the pristine $MAPbI_3$-based champion cell, the PCE of the BHT-$MAPbI_3$-based champion cell was increased from 12.16% to 16.88%. After storage at constant humidity of 30% for 698 h, the unpackaged $MAPbI_3$-based cell dropped rapidly, while the unpackaged BHT-$MAPbI_3$-based cell still maintained its initial conversion efficiency of 99.3%. In addition, BHT can also significantly improve the long-term stability of the device. We hope this work will provide a reference strategy for improving the efficiency and stability of perovskite solar cells.

Declaration of competing interest

The authors declare no conflict of interest.

Acknowledgments

The authors appreciate the financial support from the National Natural Science Foundation of China (Nos. 22169022, 22162026 and 62104137), the Shaanxi Technical Innovation Guidance Project of China (No. 2018HJCG-17), and the China National Postdoctoral Program for Innovative Talents (No. BX2021173), the China Postdoctoral Science Foundation (No. 2021M702058).

Supplementary materials

Supplementary material associated with this article can be found, in the online version, at doi:10.1016/j.cclet.2022.107933.

References

[1] X. Zhang, P. Tian, H. Chen, et al., Mater. Res. Bull. 129 (2020) 110918.
[2] I. Mathews, S. Sofia, E. Ma, et al., Joule 4 (2020) 822–839.
[3] M. Sun, J. Shu, C. Zhao, et al., ACS Appl. Mater. Interfaces 14 (2022) 13352–13360.
[4] Q. Zhuang, H. Wang, C. Zhang, et al., Nano Res. 15 (2022) 5114–5122.
[5] W. Yu, X. Sun, M. Xiao, et al., Nano Res. 15 (2022) 85–103.
[6] T. Hu, F. Zhang, H. Yu, et al., Nano Res. 14 (2021) 3864–3872.
[7] A. Kojima, K. Teshima, Y. Shirai, et al., J. Am. Chem. Soc. 131 (2009) 6050–6051.
[8] M. Kim, J. Jeong, H. Lu, et al., Science 375 (2022) 302–306.
[9] K. Domanski, J.P. Correa-Baena, N. Mineet, et al., ACS Nano 10 (2016) 6306–6314.
[10] C. Otero-Martínez, N. Fiuza-Maneiro, L. Polavarapu, ACS Appl. Mater. Interfaces 14 (2022) 34291–34302.
[11] Z. Ku, Y. Rong, M. Xu, et al., Sci. Rep. 3 (2013) 3132.
[12] G. Zhang, P. Xie, Z. Huang, et al., Adv. Funct. Mater. 31 (2021) 2011187.
[13] Z. Wu, Z. Liu, Z. Hu, et al., Adv. Mater. 31 (2019) 1804284.
[14] G.J.A.H. Wetzelaer, M. Scheepers, A.M. Sempere, et al., Adv. Mater. 27 (2015) 1837–1841.
[15] B. Chen, P.N. Rudd, S. Yang, et al., Chem. Soc. Rev. 48 (2019) 3842–3867.
[16] Z. Liu, L.K. Ono, Y. Qi, J. Energy Chem. 46 (2020) 215–228.
[17] L. Fu, H. Li, L. Wang, et al., Energy Environ. Sci. 13 (2020) 4017–4056.
[18] R. Wang, J. Xue, K.L. Wang, et al., Science 366 (2019) 1509–1513.
[19] J. Zhou, M. Li, S. Wang, et al., Nano Energy 95 (2022) 107036.
[20] Y. Cheng, Q. Wei, Z. Ye, et al., Sol. RRL 6 (2022) 2200418.
[21] K. Zhu, S. Cong, Z. Lu, et al., J. Power Sources 428 (2019) 82–87.
[22] L. Xie, J. Chen, P. Vashishtha, et al., ACS Energy Lett. 4 (2019) 2192–2200.
[23] G. Liu, H. Zheng, L. Zhang, et al., Chem. Eng. J. 407 (2021) 127204.
[24] S. Qiu, X. Xu, L. Zeng, et al., J. Energy Chem. 54 (2021) 45–52.
[25] Y. Li, Z. Chen, B. Yu, et al., Joule 6 (2022) 676–689.
[26] M.R. Tamayo, M. Moral, A.J. Pérez-Jiménez, et al., J. Phys. Chem. C 120 (2016) 22627–22634.
[27] A. Cacciuto, S. Auer, D. Frenkel, et al., Nature 428 (2004) 404–406.
[28] M.A. Afroz, N. Ghimire, K.M. Reza, et al., ACS Appl. Energy Mater. 3 (2020) 2432–2439.
[29] M.A. Afroz, R. Garai, R.K. Gupta, et al., ACS Appl. Energy Mater. 4 (2021) 10468–10476.
[30] D. Wei, H. Huang, P. Cui, et al., Nanoscale 11 (2019) 1228–1235.
[31] M.E. Kayesh, K. Matsuishi, R. Kaneko, et al., ACS Energy Lett. 4 (2019) 278–284.
[32] D. Bi, P. Gao, R. Scopelliti, et al., Adv. Mater. 28 (2016) 2910–2915.

[33] N.K. Noel, A. Abate, S.D. Stranks, et al., ACS Nano 8 (2014) 9815–9821.
[34] F. Liu, Q. Dong, M.K. Wong, et al., Adv. Energy Mater. 6 (2016) 1502206.
[35] L. Zhao, Q. Li, C.H. Hou, et al., J. Am. Chem. Soc. 144 (2022) 1700–1708.
[36] C. Fei, B. Li, R. Zhang, et al., Adv. Energy Mater. 7 (2017) 1602017.
[37] J. Fu, K. Sun, K. Sun, et al., J. Mater. Chem. C 6 (2018) 11519–11524.
[38] C. Müller, T. Glaser, M. Plogmeyer, et al., Chem. Mater. 27 (2015) 7835–7841.
[39] W.A. Saidi, J.J. Choi, et al., J. Chem. Phys. 145 (2016) 144702.
[40] B.E. Cohen, T. Binyamin, T. Ben-Tzvi, et al., ACS Energy Lett. 7 (2022) 217–225.
[41] X. Li, W. Sheng, X. Duan, et al., ACS Appl. Mater. Interfaces 14 (2022) 34161–34170.
[42] W. Zhang, L. He, D. Tang, et al., Sol. RRL 4 (2020) 2000376.
[43] Y. Miao, G. Sathiyanx, H. Wang, et al., Chem. Eng. J. 426 (2021) 131358.
[44] H. Jiang, Z. Yan, H. Zhao, et al., ACS Appl. Energy Mater. 1 (2018) 900–909.
[45] M.J. Choi, Y.S. Lee, I.H. Cho, et al., Nano Energy 71 (2020) 104639.
[46] J. Wang, K. Liu, L. Ma, et al., Chem. Rev. 116 (2016) 14675–14725.
[47] J. Fu, K. Sun, K. Yang, et al., J. Mater. Chem. C 6 (2018) 11519–11524.
[48] J. Zhong, J. Yu, L. Cao, et al., Nano Res. 13 (2020) 1780–1786.
[49] L. Meng, C. Sun, R. Wang, et al., J. Am. Chem. Soc. 140 (2018) 17255–17262.
[50] X. Wang, W. Sun, Y. Tu, et al., Chem. Eng. J. 446 (2022) 137416.
[51] X. Zhu, S. Yang, Y. Cao, et al., Adv. Energy Mater. 12 (2022) 2103491.
[52] M. Wang, Y. Zhao, X. Jiang, et al., Joule 6 (2022) 1032–1048.
[53] H. Ma, M. Wang, Y. Wang, et al., Chem. Eng. J. 442 (2022) 136291.
[54] E. Jokar, C.H. Chien, A. Fathi, et al., Energy Environ. Sci. 11 (2018) 2353–2362.
[55] H. He, X. Gao, K. Xu, et al., Chem. Eng. J. 450 (2022) 138266.
[56] C.Y. Chang, C.Y. Chu, Y.C. Huang, et al., ACS Appl. Mater. Interfaces 7 (2015) 4955–4961.
[57] T. Ye, Y. Hou, A. Nozariasbmarz, et al., ACS Energy Lett. 6 (2021) 3044–3052.
[58] W. Dong, W. Qiao, S. Xiong, et al., Nano-Micro Lett. 14 (2022) 108.